Experimental study of the $3^3\Pi_g$ and $4^3\Sigma_g^+$ states of the rubidium dimer

P. T. Arndt, V. B. Sovkov, J. Ma, X. Pan, D. S. Beecher, J. Y. Tsai, R. Livingston, V. M. Marcune, A. M. Lyyra, and E. H. Ahmed

Experimental Study of the $3^3\Pi_g$ and $4^3\Sigma_g^+$ States of Rubidium Dimer

P. T. Arndt[1], V. B. Sovkov[2,3], J. Ma[3,4], X. Pan[1], D. S. Beecher[1], J. Y. Tsai[1], R. Livingston[1], V. M. Marcune[1], A. M. Lyyra[1], and E. H. Ahmed[1,*]

[1]*Physics Department, Temple University, Philadelphia, PA 19122, USA*

[2] *St. Petersburg State University, 7/9 Universitetskaya nab., St. Petersburg 199034, Russia*

[3] *State Key Laboratory of Quantum Optics and Quantum Optics Devices, Institute of Laser Spectroscopy, College of Physics and Electronics, Shanxi University, Taiyuan 030006, China*

[4]*Collaborative Innovation Center of Extreme Optics Shanxi University Taiyuan, Shanxi 030006, People's Republic of China*

This paper reports a high-resolution experimental study of the $3^3\Pi_g$ and $4^3\Sigma_g^+$ electronic states of $^{85}Rb_2$ dimer. In the experiment, ro-vibrational levels of the two electronic states were probed using the perturbation facilitated optical-optical double resonance (PFOODR) technique by exciting $^{85}Rb_2$ molecules from thermally populated levels of the ground $X^1\Sigma_g^+$ state through intermediate levels of the mixed $A^1\Sigma_u^+ \sim b^3\Pi_u$ electronic states. The resonances of the probe laser were observed by detecting the laser induced fluorescence (LIF) from the target states to the $a^3\Sigma_u^+$ triplet ground state. In addition, to confirm the triplet character as well as the vibrational quantum number assignment of the states, for selected resonances the fluorescence to the $a^3\Sigma_u^+$ state was resolved and bound-free spectra were recorded. From the observed term values for each state potential energy curves were constructed using the Rydberg-Klein-Rees (RKR) method.

*Author to whom correspondence should be addressed.
email: erahmed@temple.edu

I. Introduction

Interatomic potentials of alkali dimers are of fundamental importance for the understanding and description, among others, of the formation of ultra-cold ground state molecules, Bose–Einstein and Fermi condensates, and ultra-cold atom-molecules collisions Refs. [1-8]. From the homonuclear alkali metal dimers the lighter Li_2 [9-23] and Na_2 [20, 24-33] molecules have been studied in most detail. A number of studies have been also devoted to the heavier K_2 dimer [34-44]. The electronic structures of the heaviest homonuclear alkali dimers Rb_2 [45-57] and Cs_2 [58-65] are less well known due to experimental difficulties associated with the relatively large densities of states as well as the presence of strong perturbations and character mixing arising from effects such as the spin-orbit interaction. There are a number of *ab initio s*tudies of the Rb_2 dimer [66-76] and even though the accuracy of such calculations has improved significantly, they are not yet suitable for direct use in experiments relying on precise knowledge of the energy of levels and transitions. Thus, experimental results on the electronic structure of the Rb_2 molecule are still highly desirable. The singlet and triplet, $X^1\Sigma_g^+$ [48, 49] and $a^3\Sigma_u^+$ [51], ground states of Rb_2 dimer as well as the electronic states arising from the first exited atomic limit ($5s+5p$) such as the $A^1\Sigma_u^+ \sim b^3\Pi_u$ [48, 50, 53] and the $B^1\Pi_u$ [47] states are well described experimentally with high accuracy. In contrast, there is only limited experimental data for the electronic states of rubidium dimer arising from higher atomic limits. Recently we have reported experimental observations of the singlet $3^1\Pi_g$ and $6^1\Sigma_g^+$ electronic states of the Rb_2 molecule [77, 78]. Building on these results in this work we extend our spectroscopic studies to the triplet $3^3\Pi_g$ and $4^3\Sigma_g^+$ states present in the same energy range of $24000 - 26000$ cm^{-1}.

II. Experiment

The experimental setup is shown in Fig. 1. It is similar to the setup used previously to study the $3^1\Pi_g$ and $6^1\Sigma_g^+$ electronic states of the Rb_2 molecule [77, 78]. Briefly, rubidium metal (Alfa Aesar 10315, 99.75%) with natural abundance ratio of the ^{85}Rb (72.17%) and ^{87}Rb (27.83%) isotopes [79] was loaded into a heat-pipe oven. Only transitions of the ^{85}Rb$_2$ isotopologue of the rubidium dimer were probed in this experiment. To contain the rubidium vapor in the center of the heatpipe oven [80] argon (Airgas UHP300, 99.999%) was used as a buffer gas at 2 Torr pressure (room temperature). The center of the heat-pipe oven was heated with electric heaters to a temperature of 180 °C producing Rb$_2$ dimer at a pressure of approximately 1.8×10^{-5} Torr [81]. From the temperature of the oven we estimate a Doppler linewidth (FWHM) for the pump transition of about 400 MHz [82].

Counter-propagating laser beams in a cascade pump-probe configuration was employed to study the 24 000 – 26 000 cm^{-1} energy region as illustrated in Fig. 2. The pump laser excited the molecules from thermally populated ro-vibrational levels of the ground $X^1\Sigma_g^+$ electronic state to an intermediate level from the $A^1\Sigma_u^+\sim b^3\Pi_u$ states manifold. The $A^1\Sigma_u^+$ and $b^3\Pi_u$ states strongly perturb each other due to their substantial spin-orbit coupling, inherited from the $5p$ atomic state with fine structure splitting of its $^2P_{1/2}$ and $^2P_{3/2}$ doublet of 237.595 cm^{-1} [83]. Thus, the ro-vibrational levels of the $A^1\Sigma_u^+\sim b^3\Pi_u$ manifold have a mixture of singlet and triplet multiplicity. This allowed us to access the triplet exited states of the rubidium molecule using the PFOODR (perturbation facilitated OODR) technique [13, 25, 84] starting from levels of the $X^1\Sigma_g^+$ ground electronic state with pure singlet character. All intermediate levels of from the $A^1\Sigma_u^+\sim b^3\Pi_u$ manifold used in the experiment nominally belong to the $A^1\Sigma_u^+$ state, the singlet multiplicity

character is the dominant component, with substantial admixture exclusively from the $b^3\Pi_{0u}$ component only.

Resolved LIF spectra from the intermediate levels to the ground $X^1\Sigma_g^+$ state were recorded with a Fourier-transform infrared spectrometer (FTIR, Bomem DA8) at a resolution of 0.01 cm^{-1}. The FTIR spectrometer was calibrated with a uranium hollow cathode lamp [85, 86]. Excitation of a specific intermediate level was confirmed by observing matching PR progressions in the resolved fluorescence spectra of the P and R branch $A^1\Sigma_u^+ - X^1\Sigma_g^+$ pump laser transitions. An example for such spectra is given in Fig. 3 for the $A^1\Sigma_u^+ \sim b^3\Pi_u(n' = 148, J = 30)$ intermediate level. In addition, the observed LIF resonances were matched with transition frequency predictions from the term values of the $X^1\Sigma_g^+$ [49] and $A^1\Sigma_u^+ \sim b^3\Pi_u$ [50] states. The label n' (not a quantum number), adopted from Ref. [50], denotes the coupled-channel vibrational eigenstates by increasing energy of the $A^1\Sigma_u^+$ and $b^3\Pi_u$ mixed electronic states. For the angular momenta and their projections on the molecular axis we follow standard notations [87]; $\vec{S}$ total electron spin with projection Σ, $\vec{L}$ electron orbital angular momentum with projection Λ, $\vec{R}$ nuclear rotational angular momentum, $\vec{J} = \vec{R} + \vec{S} + \vec{L}$ total orbital angular momentum excluding nuclear spin with projection $\Omega = \Sigma + \Lambda$, and $\vec{N} = \vec{R} + \vec{L}$ with projection Λ.

The resonances to the $3^3\Pi_g$ and $4^3\Sigma_g^+$ states were observed by detecting LIF emission to the $a^3\Sigma_u^+$ state in the 480–520 nm range using a photomultiplier tube (PMT, R928P Hamamatsu Photonics) attached to one of the side arms of the heat-pipe. Color filters (Kopp Glass 4303 and 4305) were used to suppress the amount of laser scatter and fluorescence outside of the wavelength range of interest reaching the PMT. The current output of the PMT was amplified with a lock-in amplifier (SR 850 Stanford Research) while the pump laser beam was repetitively switched on and

off at frequency of approximately 1 kHz using rotating chopper (SR540 Stanford Research). The probe laser was scanned continuously in the energy range of 13300 – 14000 cm^{-1}, calibrated using the iodine atlas [88, 89] in a similar fashion as described in ref. [77], while the amplified output of the PMT detector was recorded as function of the laser frequency. The iodine signal was amplified using a lock-in amplifier (SR 850) in the same fashion as the LIF signal. A large number of resonances, with many of them accidental, were observed in each probe laser scan due to the high density of ro-vibrational levels in the rubidium molecule. To distinguish the probe laser resonances originating from the specific target $A^1\Sigma_u^+ \sim b^3\Pi_u(n',J')$ intermediate level from all other resonances each probe laser scan was acquired twice with the pump laser at $A^1\Sigma_u^+ \sim b^3\Pi_u(n',J') \leftarrow X^1\Sigma_g^+(v'',J'+1)$ and $A^1\Sigma_u^+ \sim b^3\Pi_u(n',J') \leftarrow X^1\Sigma_g^+(v'',J'-1)$ transitions, respectively. Only the probe laser resonances observed at the same frequency with similar intensity and line shape for both pump branches were considered as originating from the $A^1\Sigma_u^+ \sim b^3\Pi_u(n',J')$ intermediate level.

In the probe laser scans vibrational progressions of two electronic states were observed with each vibrational transition containing P and R rotational branches. From the mixed $A^1\Sigma_u^+ \sim b^3\Pi_u$ intermediate levels excitations to singlet as well as triplet states are possible. To determine the electron spin multiplicity of the excited states bound-free fluorescence [90] from selected ro-vibrational levels to the repulsive part of the $a^3\Sigma_u^+$ state potential was recorded at resolution of ~ 0.75 nm using a SPEX 1404 grating spectrometer with fully open (3 mm width) slits. The LIF from the side arm of the heat-pipe was directed, with the aid of a set of mirrors and lenses, to the entrance slit of the spectrometer. The spectra were recorded by scanning the spectrometer while the pump and probe laser were held on resonance. An example spectrum illustrating the structure and origin of the observed bound-free fluorescence is given in Fig. 4.

Well-developed oscillatory fluorescence features [90, 91] were observed in the recorded spectra of the $3^3\Pi_g$ and $4^3\Sigma_g^+$ states (see Fig. 5), a clear indication of a triplet spin multiplicity. In contrast, this is not the case for singlet states, as the transitions to the $a^3\Sigma_u^+$ state are not directly allowed and instead the bound-free fluorescence arises due to coupling and collisional transfer with nearby excited triplet states. An additional important application of the observed bound-free spectra was their use in assignment of the vibrational quantum number for the observed levels by counting the nodes [90] present in each spectrum. Using *ab initio* predictions [76] in conjunction with the electronic and rotational transition selection rules for diatomic molecules [92] applied to the triplet $b^3\Pi_{0u}$ component of the mixed intermediate levels, the two observed states were identified as the $3^3\Pi_g$ and $4^3\Sigma_g^+$ electronic states. A good representation for the $^3\Pi$ states of Rb$_2$ is Hund's case (a) [93]. Thus, on account of the $\Delta\Sigma = 0$ selection rule the probe transitions observed for the $3^3\Pi_g$ state must be to its $\Omega = 0$ ($\Delta\Omega = \Delta\Sigma + \Delta\Lambda = 0$) component ($3^3\Pi_{0g} \leftarrow A^1\Sigma_u^+ \sim b^3\Pi_{0u}$). This is further corroborated by the absence of weak Q branch transitions in our spectra. In Hund's case (a) $^3\Pi_0 \leftarrow {}^3\Pi_0$ transitions have only P and R branches, while $^3\Pi_1 \leftarrow {}^3\Pi_1$ and $^3\Pi_2 \leftarrow {}^3\Pi_2$ transitions in addition exhibit a weak Q branch [92].

In addition to the direct probe laser resonances, a number of collisional satellites (see Fig. 6) as described in previous experiments in heat-pipe ovens [94-96], were observed. In our case the satellite lines occur because of inelastic J changing collisions between Rb$_2$ molecules excited to the intermediate level and argon or rubidium atoms present in the heat-pipe. A spectrum observed due to collisionally induced transfer between levels, in general, is a result of an ensemble average of binary collisions with statistical distribution of parameters such as the relative collision velocity and initial orientation of the colliding partners. Thus, the rules for transitions between levels of a molecule arising from collisions with other atoms or molecules lack the rigor of radiative

transitions. Nevertheless, by considering the symmetry of the initial and final states, propensity rules often can be obtained. In the discussion bellow we derive propensity rule for the J-changing collisions observed in our experiment by following the general analysis given in Refs. [87, 92]. The ^{85}Rb nuclei are fermions with nuclear spin of $5/2$. Therefore, the total molecular wave function ψ_{total} of the ^{85}Rb$_2$ molecule must be antisymmetric (Pauli exclusion principle) under the action of the nuclei exchange operator P_{12}, i.e., $P_{12}\psi_{\text{total}} = -\psi_{\text{total}}$. In most cases it is possible write $\psi_{\text{total}} = \psi\psi_{\text{ns}}$, where ψ_{ns} is the nuclear spin component of the total wavefunction and ψ contains all other, such as electron spin, orbital, vibrational, and rotational, components. The possible values of the total nuclear spin, I, for the ^{85}Rb$_2$ molecule are 5, 4, 3, 2, 1, and 0. The *ortho* nuclear spin configurations ($I = 5, 3, 1$ and statistical weight $g = 21$) have symmetric ψ_{ns} function, while the *para* nuclear spin configurations ($I = 4, 2, 0$ and statistical weight $g = 15$) have antisymmetric ψ_{ns}. When we consider P_{12} acting only on ψ we have $P_{12}\psi = \pm\psi$, where the symmetric $+$ states are labeled as s and the antisymmetric $-$ states are labeled as a. The symmetry of the rotational levels of the $A^1\Sigma_u^+$ state, the dominant character of the intermediate levels used in the experiment, alternate with J (even J levels have a symmetry and odd J levels s symmetry) [87]. Therefore, for ψ_{total} to be antisymmetric the rotational levels of the $A^1\Sigma_u^+$ state with a symmetry (even J) must be associated with *ortho* nuclear spin states and conversely s symmetry rotational levels (odd J levels) must be associated with *para* nuclear spin configurations. Selection rules stipulate that the total symmetry (parity) of the molecule must be rigorously preserved during transitions, including transitions arising from collisions. Collisions that change the nuclear spin symmetry are rare [92, 97] indicating that the symmetry of ψ is preserved during most collisions. Therefore, during collisions a propensity for symmetric–symmetric ($s \leftrightarrow s$) and antisymmetric–antisymmetric ($a \leftrightarrow a$) transfer exists while transfer between symmetric and

7

antisymmetric states ($s \leftrightarrow a$) are strongly suppressed (see page 131 of ref. [92]). From this follows that only even J changing collisional satellite lines, $\Delta J = \pm 2, \pm 4, ...$, will be observed in the experiment. The collisional lines enhance the rotational data acquired for each observed vibrational level of the two electronic states. The steps in the procedure of assigning their rotational quantum numbers are discussed in detail in ref. [78].

III. Results and Analysis

The $3^3\Pi_g$ and $4^3\Sigma_g^+$ states of the Rb$_2$ molecule lie in an energy region with high density of electronic states (see Fig. 2) as predicted by *ab initio* calculations [75, 76] and previous experimental observations [77, 78]. The interactions between the electronic states of *gerade* symmetry $3^1\Pi_g$, $5^1\Sigma_g^+$, $6^1\Sigma_g^+$, $3^3\Pi_g$, and $4^3\Sigma_g^+$ in this range cause perturbations of their rovbrational levels. In addition, a*b initio* predictions indicate especially strong interactions between these states around 26000 cm^{-1} which become evident by the unusual features such as avoided crossings and secondary wells present in their adiabatic potential curves. Nevertheless, in our experimental observations we were able to discern two vibrational progressions which we have assigned to the $3^3\Pi_g$ and $4^3\Sigma_g^+$ electronic states. The ro-vibrational energy data observed in the experiments for the $3^3\Pi_g$ and $4^3\Sigma_g^+$ states is illustrated in Fig. 7. The rotational quantum numbers in the plots, J for the $3^3\Pi_g$ state (Hund's case (a)) and N for the $4^3\Sigma_g^+$ state (Hund's case (b)), were derived from the rotational quantum number of the intermediate level $A^1\Sigma_u^+ \sim b^3\Pi_u(n', J')$ for the P and R probe laser excitation branches as J (or N) $= J' - 1$ and J (or N) $= J' + 1$, respectively. The term energy of each of the observed levels along with details of the excitation pathways used to access them are given in the supplementary materials at {*URL will be inserted by publisher*}.

The vibrational quantum number is typically very difficult to obtain in this type of spectroscopic studies due to the lack of selection rules for vibrational transitions. Nevertheless, in this case we were able to create assignment for the vibrational quantum numbers of the observed levels from the experimentally measured bound-free spectra presented in Fig. 5. An unusual behavior in the bound-free spectra is observed going from $v = 3$ to $v = 4$ for the $3^3\Pi_g$ state (see Fig. 5) where one of the nodes vanishes and the node count for the vibrational levels with $v \geq 4$ is $v - 1$. Similarly, a node vanishes in the bound-free spectra of the $4^3\Sigma_g^+$ state going from $v = 16$ to $v = 17$. There are several possible causes for such puzzling behavior, but none appear to give satisfactory explanation. For example, if a shelf or second minimum develops in the potential curve, it will strongly affect the bound-free spectrum due to an onset of sampling at longer R range of the upper state ro-vibrational wave function. We believe this is not likely in our case since the observed vibrational spacing is not consistent with shelf or second minimum region. Moreover, these features are not present in the corresponding energy range of either the *ab initio* curves of Ref. [76] or the experimental potential curves derived in this work. Another possible cause is a rapid decrease in the electronic transition dipole moment function of the upper states to the $a^3\Sigma_u^+$ state in a relatively narrow R range near R_e, where the large momentum of the molecules results in closely spaced nodes. Then, the combination of low amplitude and close spacing can lead to unresolved node in the experimental bound-free spectra. Unfortunately, we cannot further explore this possibility since the transition dipole moment functions of the $3^3\Pi_g$ and $4^3\Sigma_g^+$ states with the $a^3\Sigma_u^+$ state are not known. In addition, no obvious low intensity range in the bound-free spectra is observed. A third alternative is an interference effect due to borrowed oscillator strength from another triplet state that has an allowed transition to the $a^3\Sigma_u^+$ state. The drawback of this hypothesis is that in our experiments no additional triplet states were observed.

The calculations described below were carried out using the computational package OPTIMIZER [98]. The main package, along with the library of application programs for quantum-mechanical simulations and analysis of molecular spectra, is freely available for download at [99]. The project OPTIMIZER is constantly being developed and expanded. In this context, we would like to mention that many of our previous analyses of alkali metal dimers also used OPTIMIZER [39, 40, 43, 51, 59, 61, 64, 77, 78, 100-102].

Following the assignments of the vibrational and rotational quantum numbers of the observed term values the data for the $3^3\Pi_g$ and $4^3\Sigma_g^+$ states were fitted by a least squares method with

$$T_{v,J} = \sum_{k,l} Y_{k,l}(v + 1/2)^k [J(J + 1) - \Omega^2 + S(S + 1) - \Sigma^2]^l \tag{1a}$$

and

$$T_{v,J} = \sum_{k,l} Y_{k,l}(v + 1/2)^k [N(N + 1) - \Lambda^2]^l, \tag{1b}$$

the Dunham expansion [103] equations for Hund's case (a) and (b) [92], respectively. A series of fits in which a balance between improvements in the fits and statistical significance of newly added constants was carried out to determine the optimum set of coefficients for each state. Considering that all the experimental results were acquired under the same conditions, equal weights were used for all data points in the fitting process. The final results of the fitting process for both states are presented in Table 1. Once the Dunham coefficients were determined the potential energy curves of the states were generated by utilizing the first-order semiclassical Rydberg-Klein-Rees (RKR) method [104-107]. The results for the turning points $R_{\min}$ and $R_{\max}$ of the potentials together with the $G_v + Y_{0,0} = \sum_k Y_{k,0}(v + 1/2)^k$ values (*i.e.*, the values of the potential energy functions relative their minima) are tabulated in Tables 2 and 3 for the $3^3\Pi_g$ and $4^3\Sigma_g^+$ states. The tables include the effective vibrational quantum numbers at the bottoms of the potential wells, $v = -0.5001$ and v =

- 0.4959 for the $3^3\Pi_g$ and $4^3\Sigma_g^+$ states, respectively. Their difference from -1/2 indicates that the Kaiser correction [108, 109] was embedded into the RKR algorithm. The RKR and *ab initio* potentials [76] for both states are plotted in Fig. 8.

Our experimental values for the molecular constants, T_e, ω_e, and B_e, are generally in line with the *ab initio* predictions as illustrated in Table 4. Nevertheless, it should be noted that the experimental B_e values are consistently smaller than the *ab initio* predictions. This is reflected in Fig. 8 where the experimental potentials are shifted to larger internuclear distance relative to the theoretical curves from Ref. [76]. We note that at the equilibrium internuclear distance of a molecular potential, R_e, and B_e are related according to the following equation [87]

$$B_e = \frac{h \times 10^{-2}}{8\pi^2 \mu c} \times \frac{1}{R_e^2}, \tag{2}$$

where B_e is in cm^{-1} units while all physical constants are in SI units. The reduced mass of the ^{85}Rb$_2$ molecule is $\mu = m(^{85}$Rb$)/2 = 7.0499797224 \times 10^{-26}$ kg (42.4558962 amu) [79]. The systematic discrepancy in R illustrated in Fig. 8 is possibly an indication of incompletely or incorrectly accounted couplings in the *ab initio* calculations. This is further corroborated by the discrepancy between the *ab initio* and RKR curves for the $3^3\Pi_g$ state above 25 300 cm^{-1}. The theoretical calculations for the $3^3\Pi_g$ predict a barrier and a secondary well. In contrast, our RKR curve in this range appears to suggest a simple broadening of the potential or the existence of a shelf.

The presence of perturbations in the observed term values is evident in the Dunham fit residuals plotted in Figs. 9 and 10 for the $3^3\Pi_g$ and $4^3\Sigma_g^+$ states, respectively. Indicative of this are the clearly observed rotational dependences of the residuals of some of the vibrational levels. This is expected for highly excited electronic states of Rb$_2$ due to the high density of states and the presence of various allowed nonadiabatic couplings. For both states the perturbations are enlarged

above 25 300 cm^{-1}. Similar perturbation enhancement has been previously observed in the same energy region for the $3^1\Pi_g$ and $6^1\Sigma_g^+$ states [77, 78]. Thus, it can be concluded that in this energy range the $3^1\Pi_g$, $6^1\Sigma_g^+$, $3^3\Pi_g$ and $4^3\Sigma_g^+$ states strongly perturb each other. The current absence of details about the interactions that cause these perturbations prevents the use of coupled-channel methods [50, 63, 65, 110, 111] for global simultaneous analysis of the perturbing states.

IV. Conclusions

We have observed a large set of ro-vibrational levels of the $3^3\Pi_g$ and $4^3\Sigma_g^+$ states of the Rb$_2$ dimer using the PFOODR technique. Well defined Condon structures were observed in the resolved bound-free fluorescence from the laser-populated upper levels to the repulsive region of the $a^3\Sigma_u^+$ state potential. This allowed us to determine the vibrational quantum number assignment of the observed states as well as to confirm their triplet character. The experimental observations reveal the presence of many perturbations in the observed energy range of the $3^3\Pi_g$ and $4^3\Sigma_g^+$ states. In addition, the strong enhancement of the perturbations around 25 300 cm^{-1} is compelling evidence for the existence of avoided crossings of potential energy curves in this range. Despite the irregularities in the observed data due to the presence of perturbations, we were able to construct potential curves for both states using the Dunham expansion and the RKR method.
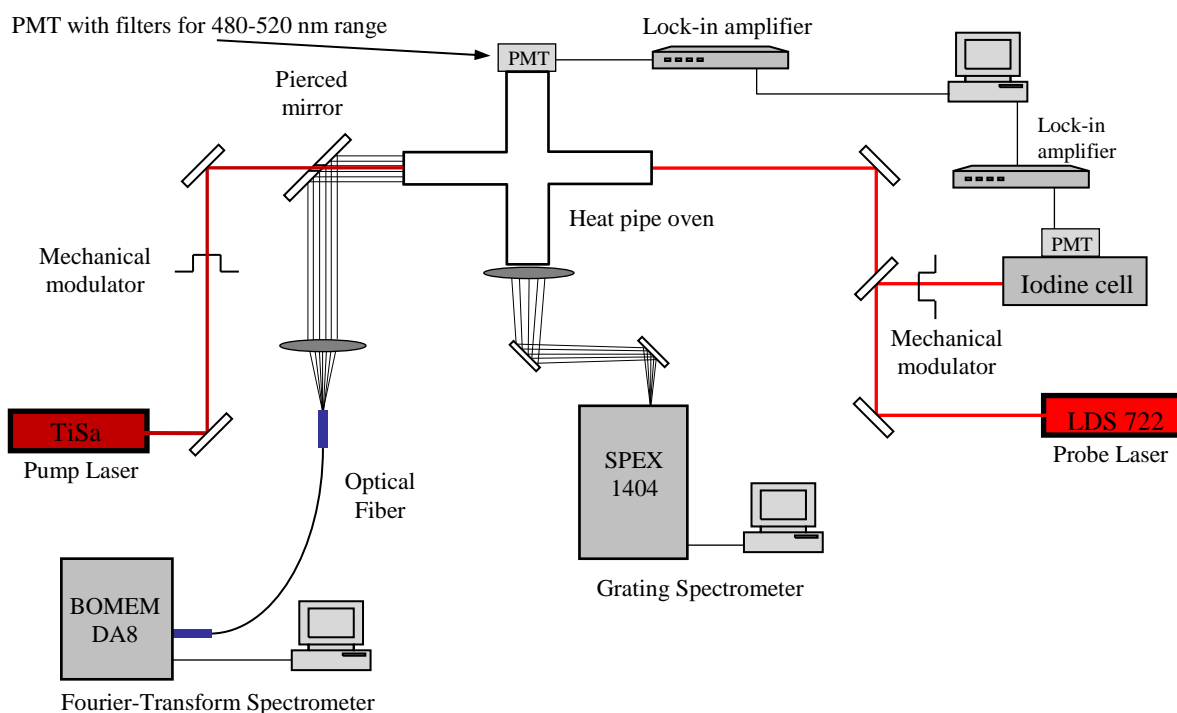
Fig. 1 Schematic diagram of the experimental set-up. Tunable cw single-mode narrow band (~1 MHz) Coherent 899-29 Titanium Sapphire (L_{pump}) and Coherent 699-29 with LDS 722 dye (L_{probe}) lasers are used as the pump and probe, respectively. L_{pump} and L_{probe} are in the counter-propagating configuration. Probe laser resonances to the $3^3\Pi_g$ and $4^3\Sigma_g^+$ states are observed by monitoring LIF to the $a^3\Sigma_u^+$ state with a photo multiplier tube (R928P Hamamatsu Photonics) detector attached to one of the side arms of the heat-pipe oven. The bound-free florescence from the $3^3\Pi_g$ and $4^3\Sigma_g^+$ states was recorded using SPEX 1404 grating spectrometer with photomultiplier tube (R928P Hamamatsu Photonics) detector.
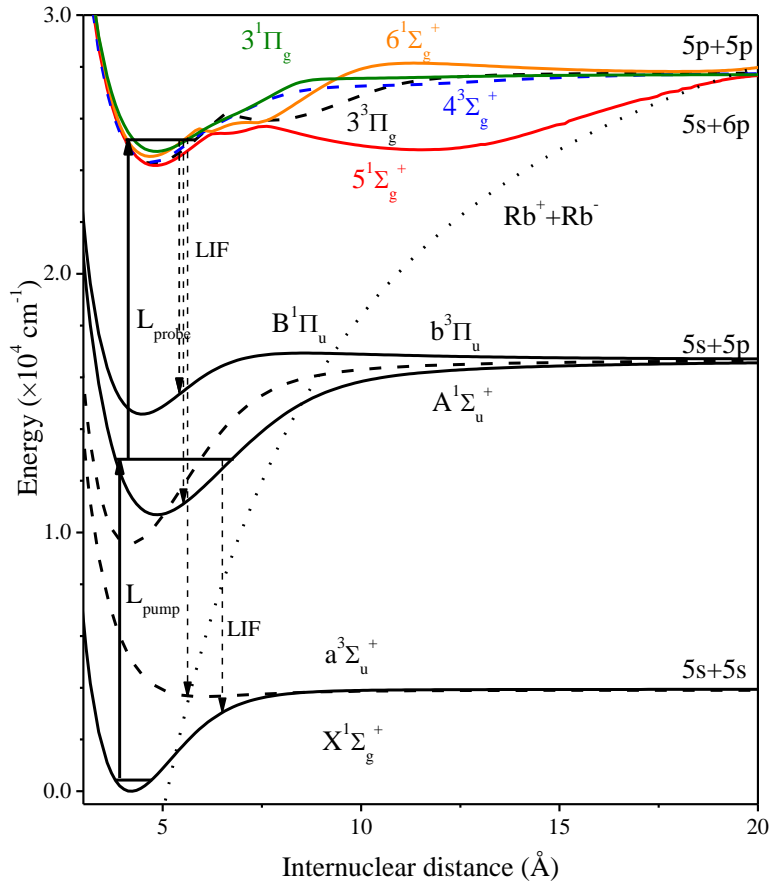
14

Fig. 2 Excitation scheme of the experiment and potential energy curves of the rubidium dimer. The pump laser excites molecules from a single thermally populated ro-vibrational level of the $X^1\Sigma_g^+$ ground electronic state to an intermediate level with a mixed multiplicity character from the $A^1\Sigma_u^+ \sim b^3\Pi_u$ manifold. The probe laser further excites these molecules to the target $3^3\Pi_g$ and $4^3\Sigma_g^+$ electronic states. The probe laser resonances are detected by monitoring the fluorescence from the $3^3\Pi_g$ and $4^3\Sigma_g^+$ states to the $a^3\Sigma_u^+$ state. The potential curves used in the figure are *ab initio* calculations from Ref. [76]. The dotted curve is the Rb$^+$+Rb$^-$ Coulomb potential energy $e^2/(4\pi\varepsilon_0 R)$.
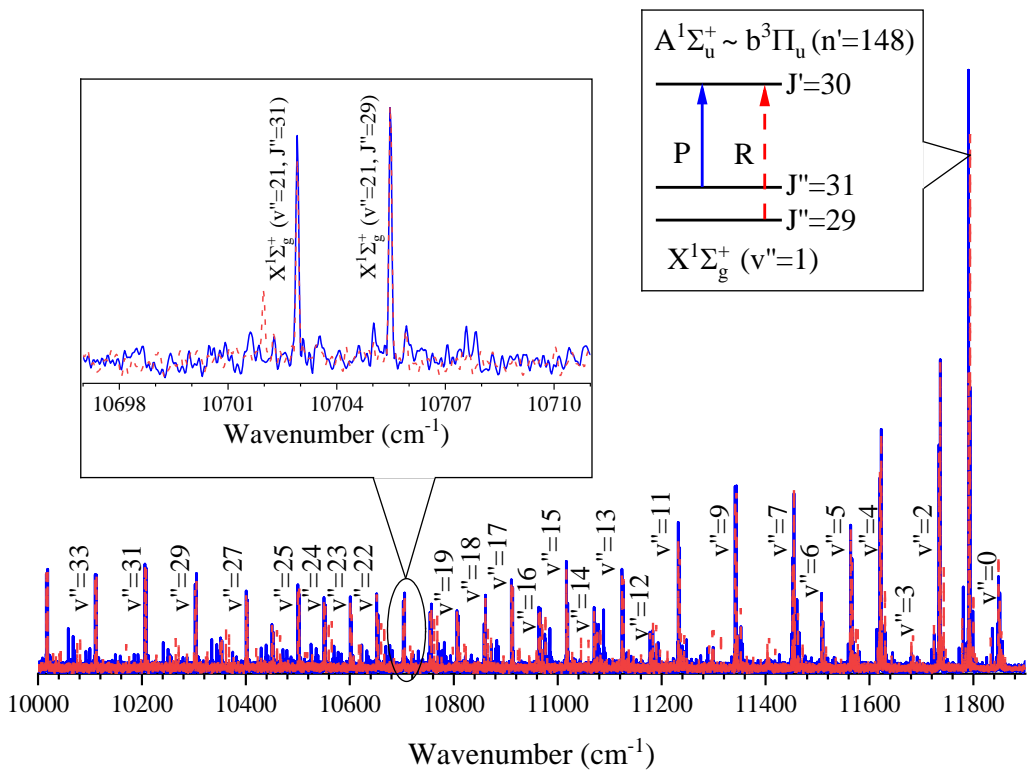
Fig. 3 Resolved LIF spectra from the $A^1\Sigma_u^+ \sim b^3\Pi_u(n' = 148, J' = 30)$ intermediate level used to confirm the pump laser *P* and *R* branch resonances. The spectra are recorded with BOMEM DA8 FTIR spectrometer. In the main panel and the insert the fluorescence from the $A^1\Sigma_u^+ \sim b^3\Pi_u(n' = 148, J' = 30) \leftarrow X^1\Sigma_g^+(v'' = 1, J'' = 31)$ and $A^1\Sigma_u^+ \sim b^3\Pi_u(n' = 148, J' = 30) \leftarrow X^1\Sigma_g^+(v'' = 1, J'' = 29)$ pump excitations are indicated with solid blue and dashed red lines, respectively.
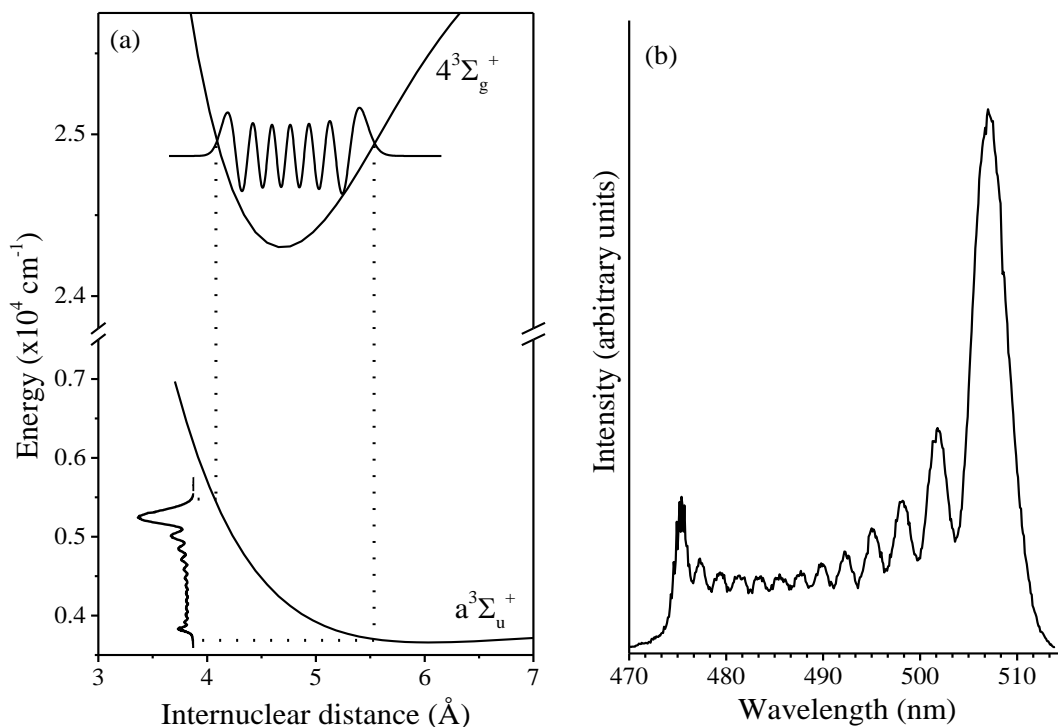
Fig. 4 Example bound-free spectrum from v = 12 of the $4^3\Sigma_g^+$ electronic state to the repulsive region of the $a^3\Sigma_u^+$ state potential. (a) The intensity of bound-free emission from a bound level to a repulsive potential on which the molecule dissociates into two free atoms is proportional to the probability distribution of the excited state wavefunction [90]. The energy range of the spectrum is determined by the term energy of the emitting level and the potential energy curve of the lower electronic state. (b) Experimentally recorded bound-free spectrum from the $4^3\Sigma_g^+(\mathrm{v} = 12, J = 11)$ level.
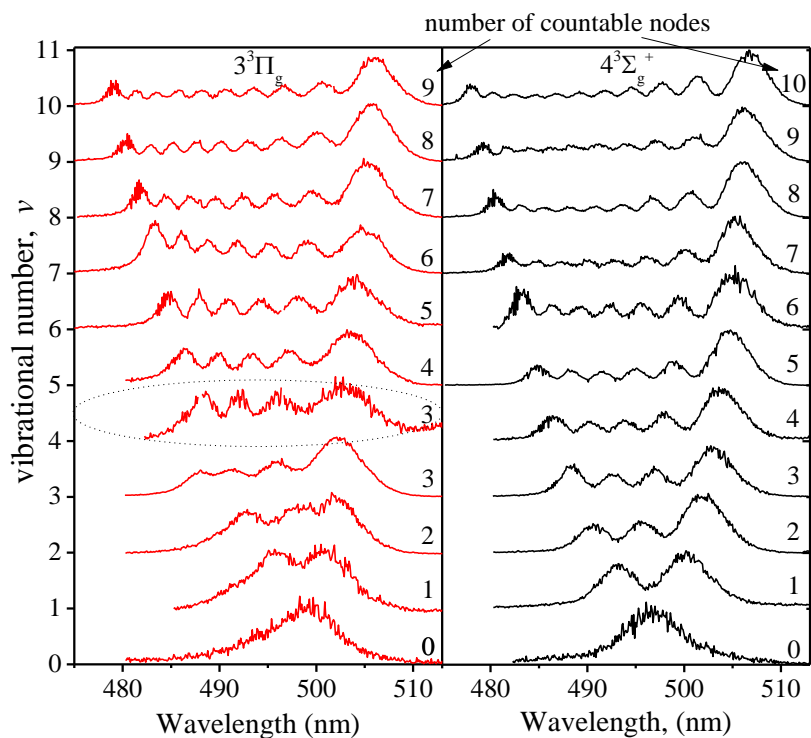
Fig. 5 The resolved bound-free emission for the first eleven vibrational levels of the $3^3\Pi_g$ (left) and the $4^3\Sigma_g^+$ (right) electronic states. The bound-free spectra for the remaining observed vibrational levels are included in the supplemental materials at {*URL will be inserted by publisher*}. The number of countable nodes is indicated on the left side of each spectrum. The bound-free spectrum ($v = 4$) of the $3^3\Pi_g$ state showing the onset of vanishing node is highlighted with dotted oval.
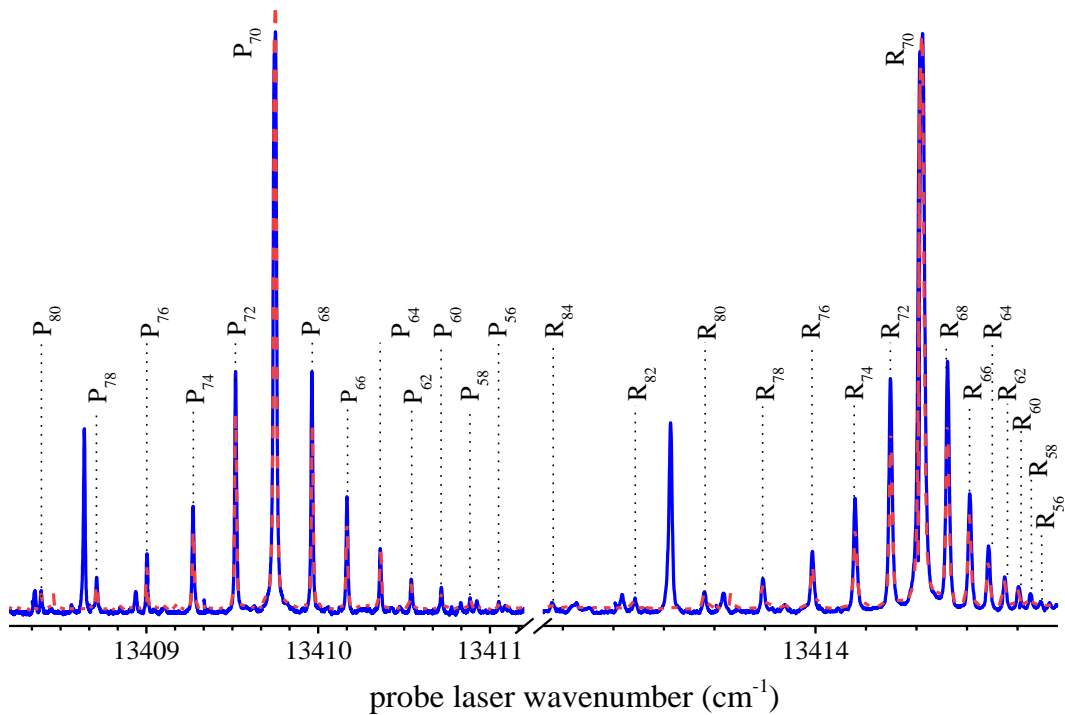
Fig. 6 A probe laser excitation spectrum of the $4^3\Sigma_g^+(v=11)$ vibrational level from the $A^1\Sigma_u^+\sim b^3\Pi_u(n'=106, J'=70)$ intermediate level. In addition to the main (parent) P_{70} and R_{70} lines, satellite lines due to collision-induced ΔJ even rotational energy transfer (RET) in the intermediate level are observed. The solid (blue) and dashed (red) trace correspond to pump laser resonant with the P_{71} and R_{69} excitations to the $A^1\Sigma_u^+\sim b^3\Pi_u(n'=106, J'=70)$ intermediate level from the $X^1\Sigma_g^+(v''=0)$ ground state vibrational level, respectively.
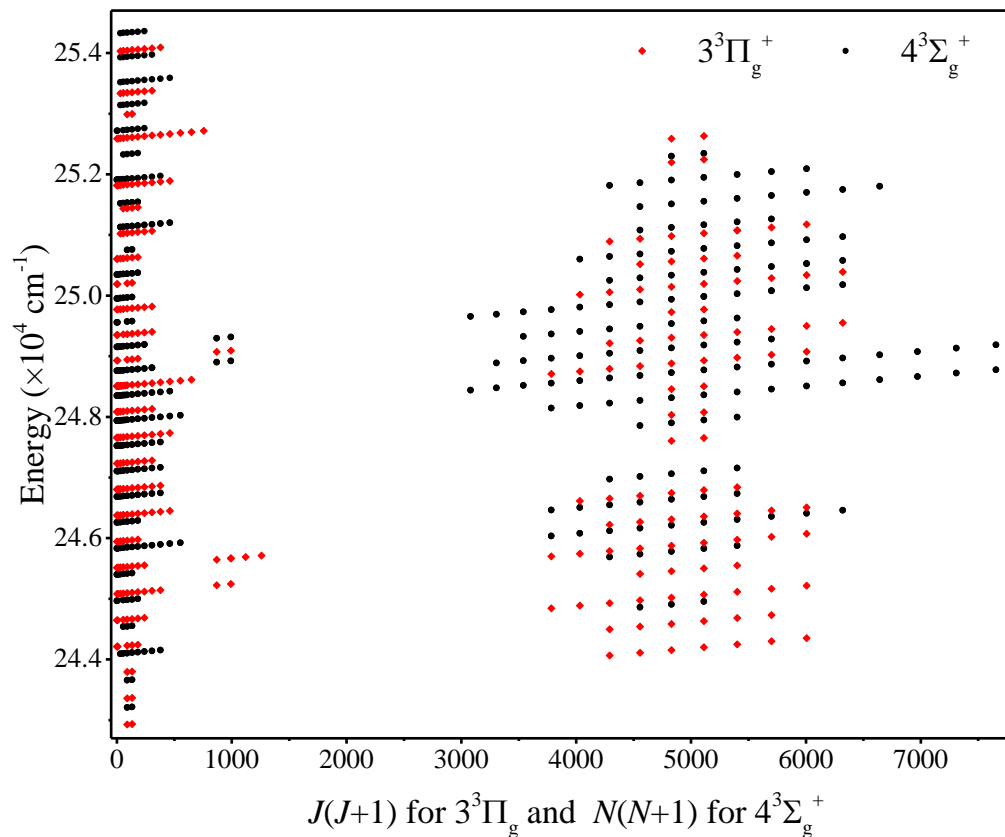
Fig. 7 The observed ro-vibrational levels of the (a) $3^3\Pi_g$ and the (b) $4^3\Sigma_g^+$ electronic states. For the $3^3\Pi_g$ state, 400 ro-vibrational levels, spanning the range of the vibrational quantum number $v = 0$ through 27 and the rotational quantum number $J = 0$ through 79. A total of 506 ro-vibrational levels in a similar range of vibrational and rotational quantum numbers were observed for the $4^3\Sigma_g^+$ state.

Fig. 8 Potential energy curves of the Rb$_2$ $3^3\Pi_g$ and $4^3\Sigma_g^+$ electronic states. The solid lines are ab initio calculations from Ref. [76] and the RKR results are represented as circles.

Fig. 9 Dunham expansion fit residuals of the observed $3^3\Pi_g$ state ro-vibrational term values.

Fig. 10 Dunham expansion fit residuals of the observed $4^3\Sigma_g^+$ state ro-vibrational term values.
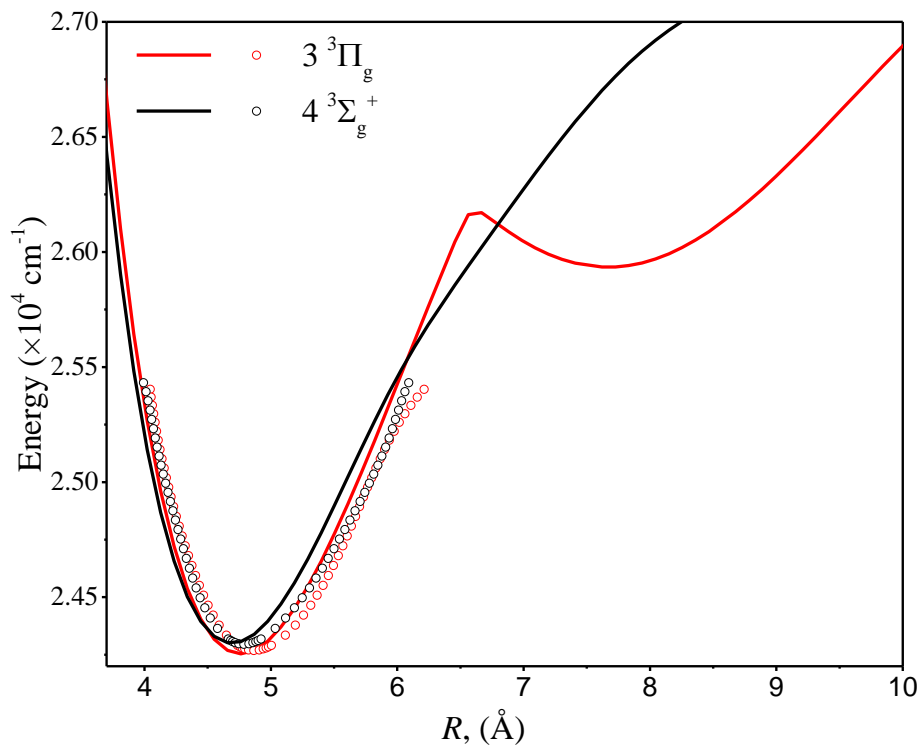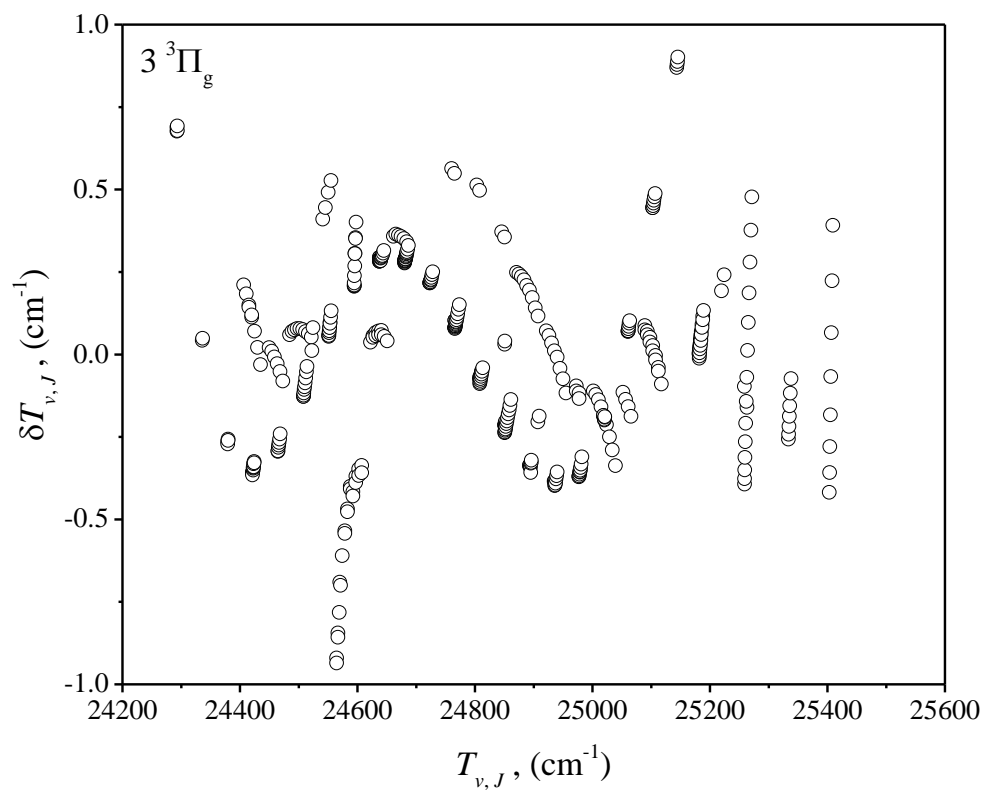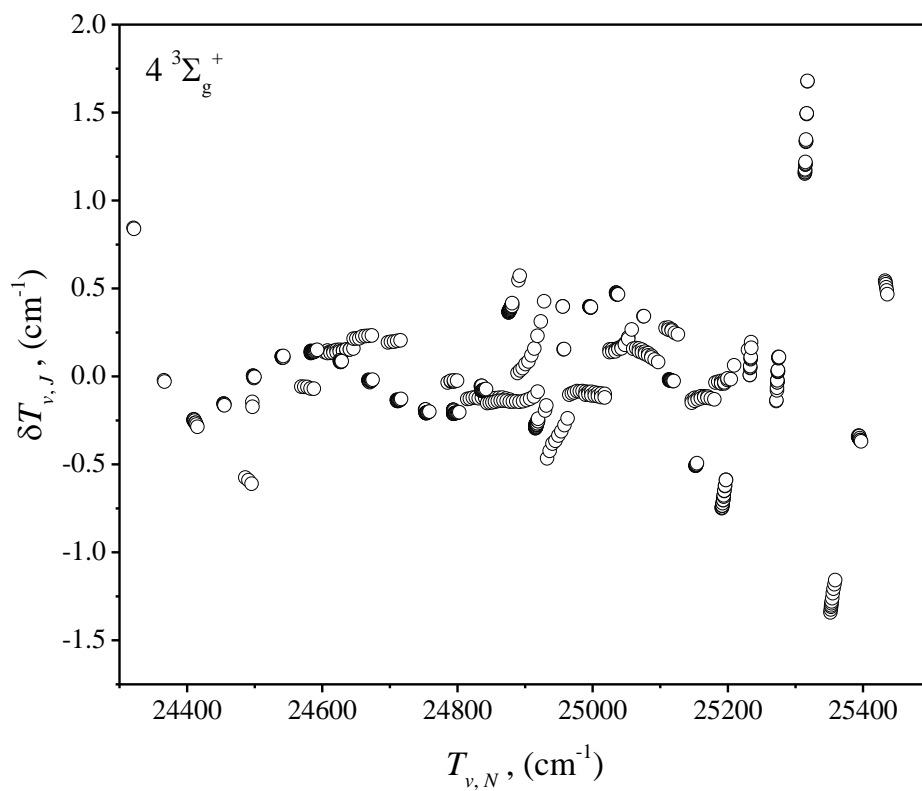
Tables

Table 1 Dunham expansion coefficients (in cm^{-1}) of the $3^3\Pi_g$ and the $4^3\Sigma_g^+$ electronic states of Rb$_2$ obtained by direct fit of the experimental data. The last two rows represent the estimates based on the approximate correlations [103, 108, 112-114]: $Y_{00}' \cong \frac{Y_{01}+Y_{20}}{4} - \frac{Y_{11}Y_{10}}{12Y_{01}} + \frac{Y_{11}^2 Y_{10}^2}{144Y_{01}^3}$ and $Y_{02}' \cong -4\frac{Y_{01}^3}{Y_{10}^2}$.

k, l	$Y_{k,l}$ for $3^3\Pi_g$	$Y_{k,l}$ for $4^3\Sigma_g^+$
$T_e + Y_{00}$	24268.409 (138)	24294.789 (349)
Y_{10}	44.2151 (561)	47.6712 (2628)
Y_{20}	-1.6451 (742) $\times 10^{-1}$	-1.04188 (6954)
Y_{30}	1.0336 (380) $\times 10^{-2}$	1.30715 (8489) $\times 10^{-1}$
Y_{40}	-3.0025 (655) $\times 10^{-4}$	-9.42103 (52195) $\times 10^{-3}$
Y_{50}		3.16996 (1569) $\times 10^{-4}$
Y_{60}		-3.93547 (18310) $\times 10^{-6}$
Y_{01}	1.6767 (62) $\times 10^{-2}$	1.7335 (59) $\times 10^{-2}$
Y_{11}	-8.79 (138) $\times 10^{-5}$	-1.101 (90) $\times 10^{-4}$
Y_{21}	8.17 (144) $\times 10^{-6}$	2.50 (37) $\times 10^{-6}$
Y_{31}	-2.730 (445) $\times 10^{-7}$	
Y_{02}	1.79 (88) $\times 10^{-8}$	-9.6 (71) $\times 10^{-9}$
Y_{00}'	0.0046 (90)	-0.1942 (191)
Y_{02}'	-9.64 (10) $\times 10^{-9}$	-9.17 (15) $\times 10^{-9}$

Table 2 RKR potential of the $3^3\Pi_g$ state generated from the Dunham coefficients listed in Table 1.

v	$R_{\min}$ (Å)	$R_{\max}$ (Å)	G_v+Y_{00} (cm^{-1})
-0.5001	R_e = 4.866349 (898) Å		0
0	4.738071	5.006532	22.072
1	4.650265	5.116445	65.990
2	4.591769	5.194927	109.664
3	4.544887	5.259856	153.140
4	4.504562	5.316479	196.460
5	4.468538	5.367252	239.656
6	4.435601	5.413597	282.755
7	4.405025	5.456452	325.775
8	4.376345	5.496502	368.727
9	4.349252	5.534280	411.617
10	4.323532	5.570225	454.442
11	4.299039	5.604717	497.190
12	4.275666	5.638097	539.846
13	4.253341	5.670675	582.385
14	4.232012	5.702747	624.774
15	4.211645	5.734596	666.975
16	4.192216	5.766498	708.943
17	4.173712	5.798730	750.623
18	4.156126	5.831570	791.955
19	4.139455	5.865302	832.872
20	4.123703	5.900224	873.299
21	4.108872	5.936648	913.153
22	4.094968	5.974909	952.346
23	4.081996	6.015372	990.780
24	4.069959	6.058439	1028.350
25	4.058861	6.104561	1064.952
26	4.048697	6.154252	1100.460
27	4.039458	6.208112	1134.752

Table 3 RKR potential of the $4^3\Sigma_g^+$ state generated from the Dunham coefficients listed in Table 1.

v	R_{min} (Å)	R_{max} (Å)	G_v+Y_{00} (cm^{-1})
-0.4959	R_e = 4.786005 (821) Å		0
0	4.663113	4.922381	23.397
1	4.578073	5.034438	69.364
2	4.521998	5.117130	114.177
3	4.478086	5.187118	158.242
4	4.441418	5.249235	201.829
5	4.409624	5.305817	245.094
6	4.381277	5.358289	288.111
7	4.355416	5.407634	330.893
8	4.331351	5.454572	373.413
9	4.308582	5.499631	415.625
10	4.286750	5.543191	457.475
11	4.265611	5.585505	498.919
12	4.245012	5.626713	539.925
13	4.224884	5.666854	580.490
14	4.205220	5.705882	620.635
15	4.186067	5.743680	660.410
16	4.167503	5.780082	699.893
17	4.149624	5.814900	739.185
18	4.132515	5.847962	778.401
19	4.116229	5.879141	817.662
20	4.100763	5.908401	857.082
21	4.086036	5.935830	896.751
22	4.071867	5.961673	936.714
23	4.057960	5.986365	976.958
24	4.043879	6.010559	1017.378
25	4.029025	6.035182	1057.754
26	4.012580	6.061510	1097.722
27	3.993417	6.091331	1136.741

Table 4 Comparisons of the experimental molecular constants of the $3^3\Pi_g$ and the $4^3\Sigma_g^+$ states with theoretical predictions. Note that the B_e values listed for ref. [75] were calculated from the R_e values given in the reference using Eq. (2).

State	T_e	ω_e	B_e	
	24268.404	44.2151	0.016767	This work
$3^3\Pi_g$	24276.5	45.6	0.01750	[76]
	24232	45.4	0.01720	[75]
	24294.983	47.6712	0.017335	This work
$4^3\Sigma_g^+$	24 323.7	46.3	0.01800	[76]
	24313	46.7	0.01770	[75]

References

1. K. K. Ni, S. Ospelkaus, M. H. G. de Miranda, A. Pe'er, B. Neyenhuis, J. J. Zirbel, S. Kotochigova, P. S. Julienne, D. S. Jin, and J. Ye, *A high phase-space-density gas of polar molecules*, Science **322**, 231 (2008). http://doi.org/10.1126/science.1163861

2. W. Salzmann, U. Poschinger, R. Wester, M. Weidemuller, A. Merli, S. M. Weber, F. Sauer, M. Plewicki, F. Weise, A. M. Esparza, L. Woste, and A. Lindinger, *Coherent control with shaped femtosecond laser pulses applied to ultracold molecules*, Phys. Rev. A **73**, 023414 (2006). http://doi.org/10.1103/PhysRevA.73.023414

3. M. H. G. de Miranda, A. Chotia, B. Neyenhuis, D. Wang, G. Quemener, S. Ospelkaus, J. L. Bohn, J. Ye, and D. S. Jin, *Controlling the quantum stereodynamics of ultracold bimolecular reactions*, Nat. Phys. **7**, 502 (2011). http://doi.org/10.1038/nphys1939

4. T. Volz, N. Syassen, D. M. Bauer, E. Hansis, S. Durr, and G. Rempe, *Preparation of a quantum state with one molecule at each site of an optical lattice*, Nat. Phys. **2**, 692 (2006). http://doi.org/10.1038/nphys415

5. J. G. Danzl, E. Haller, M. Gustavsson, M. J. Mark, R. Hart, N. Bouloufa, O. Dulieu, H. Ritsch, and H.-C. Naegerl, *Quantum gas of deeply bound ground state molecules*, Science **321**, 1062 (2008). http://doi.org/10.1126/science.1159909

6. T. M. Rvachov, H. Son, A. T. Sommer, S. Ebadi, J. J. Park, M. W. Zwierlein, W. Ketterle, and A. O. Jamison, *Long-Lived Ultracold Molecules with Electric and Magnetic Dipole Moments*, Phys. Rev. Lett. **119**, 143001 (2017). http://doi.org/10.1103/PhysRevLett.119.143001

7. C. Gross and I. Bloch, *Quantum simulations with ultracold atoms in optical lattices*, Science **357**, 995 (2017). http://doi.org/10.1126/science.aal3837

8. B. Yan, S. A. Moses, B. Gadway, J. P. Covey, K. R. A. Hazzard, A. M. Rey, D. S. Jin, and J. Ye, *Observation of dipolar spin-exchange interactions with lattice-confined polar molecules*, Nature **501**, 521 (2013). http://doi.org/10.1038/nature12483

9. P. Kusch and M. M. Hessel, *An analysis of $A^1\Sigma_u^+$-$X^1\Sigma_g^+$ band system of $^7Li_2$*, Journal of Chemical Physics **67**, 586 (1977). http://doi.org/10.1063/1.434858

10. M. E. Koch, W. C. Stwalley, and C. B. Collins, *Observation of bound-free-bound triplet absorption-bands in Li_2*, Phys. Rev. Lett. **42**, 1052 (1979). http://doi.org/10.1103/PhysRevLett.42.1052

11. R. A. Bernheim, L. P. Gold, P. B. Kelly, C. Tomczyk, and D. K. Veirs, *A spectroscopic study of the $E\ ^1\Sigma_g^+$ and $F\ ^1\Sigma_g^+$ states of $^7Li_2$ by pulsed optical–optical double resonance*, Journal of Chemical Physics **74**, 3249 (1981). http://doi.org/10.1063/1.441529

12.   R. A. Bernheim, L. P. Gold, P. B. Kelly, T. Tipton, and D. K. Veirs, *A spectroscopic study of the $G\,^1\Pi_g$ state of $^7Li_2$ by pulsed optical–optical double resonance*, Journal of Chemical Physics **74**, 2749 (1981). http://doi.org/10.1063/1.441444

13.   R. A. Bernheim, L. P. Gold, and T. Tipton, *Rydberg states of $^7Li_2$ by pulsed optical–optical double resonance spectroscopy: Molecular constants of $^7Li_2^+$*, Journal of Chemical Physics **78**, 3635 (1983). http://doi.org/10.1063/1.445192

14.   X. B. Xie and R. W. Field, *The $^6Li_2\,A\,^1\Sigma_u^+ \sim b\,^3\Pi_u$ Spin-Orbit Perturbations: Sub-Doppler Spectra and Steady-State Kinetic Lineshape Model*, Chemical Physics **99**, 337 (1985). http://doi.org/10.1016/0301-0104(85)80130-0

15.   B. Barakat, R. Bacis, F. Carrot, S. Churassy, P. Crozet, F. Martin, and J. Verges, *Extensive analysis of the $X^1\Sigma_g^+$ ground state of $^7Li_2$ by laser-induced fluorescence Fourier transform spectrometry*, Chemical Physics **102**, 215 (1986). http://doi.org/10.1016/0301-0104(86)85133-3

16.   R. A. Bernheim, L. P. Gold, C. A. Tomczyk, and C. R. Vidal, *Spectroscopic study of the $E\,^1\Sigma_g^+$ ''shelf'' state in $^7Li_2$*, Journal of Chemical Physics **87**, 861 (1987). http://doi.org/10.1063/1.453293

17.   L. Li, T. An, T. J. Whang, A. M. Lyyra, W. C. Stwalley, R. W. Field, and R. A. Bernheim, *Hyperfine Splitting of the $1^3\Delta_g$ Rydberg State of $^7Li_2$*, Journal of Chemical Physics **96**, 3342 (1992). http://doi.org/10.1063/1.461930

18.   A. Yiannopoulou, K. Urbanski, A. M. Lyyra, L. Li, B. Ji, J. T. Bahns, and W. C. Stwalley, *Perturbation Facilitated Optical-Optical Double-Resonance Spectroscopy of the $2\,^3\Sigma_g^+$, $3\,^3\Sigma_g^+$, and $4\,^3\Sigma_g^+$ Rydberg States of $^7Li_2$*, Journal of Chemical Physics **102**, 3024 (1995). http://doi.org/10.1063/1.468612

19.   K. Urbanski, S. Antonova, A. Yiannopoulou, A. M. Lyyra, and W. C. Stwalley, *All optical triple resonance spectroscopy of the $A\,^1\Sigma_u^+$ state of $^7Li_2$*, J. Chem. Phys. **104**, 2813 (1996). http://doi.org/10.1063/1.471105

20.   L. Li and A. M. Lyyra, *Triplet states of Na_2 and Li_2 by perturbation facilitated optical-optical double resonance spectroscopy*, Spectroc. Acta Pt. A-Molec. Biomolec. Spectr. **55**, 2147 (1999). http://doi.org/10.1016/s1386-1425(99)00091-8

21.   S. Antonova, G. Lazarov, K. Urbanski, A. M. Lyyra, L. Li, G. H. Jeung, and W. C. Stwalley, *Predissociation of the $F(4)^1\Sigma_g^+$ state of Li_2*, Journal of Chemical Physics **112**, 7080 (2000). http://doi.org/10.1063/1.481335

22.   W. Jastrzebski, A. Pashov, and P. Kowalczyk, *The $E\,^1\Sigma_g^+$ state of lithium dimer revised*, Journal of Chemical Physics **114**, 10725 (2001). http://doi.org/10.1063/1.1374927

23. P. Yi, M. Song, Y. M. Liu, A. M. Lyyra, and L. Li, *New pair of $A^1\Sigma_u^+ \sim b^3\Pi_u$ mixed levels in Li_6Li_7*, Chemical Physics Letters **349**, 426 (2001). http://doi.org/10.1016/s0009-2614(01)01236-2

24. P. Kusch and M. M. Hessel, *An analysis of the $B\,^1\Pi_u$–$X\,^1\Sigma_g^+$ band system of Na_2*, Journal of Chemical Physics **68**, 2591 (1978). http://doi.org/10.1063/1.436117

25. L. Li and R. W. Field, *Direct observation of high-lying $^3\Pi_g$ states of the sodium molecule by optical-optical double resonance*, Journal of Physical Chemistry **87**, 3020 (1983). http://doi.org/10.1021/j100239a011

26. O. Babaky and K. Hussein, *The ground state $X\,^1\Sigma_g^+$ of Na_2*, Canadian Journal of Physics **67**, 912 (1989). http://doi.org/10.1139/p89-157

27. L. Li, Q. S. Zhu, and R. W. Field, *The Hyperfine-Structure of the Na_2 $4\,^3\Sigma_g^+$ State*, Mol. Phys. **66**, 685 (1989). http://doi.org/10.1080/00268978900100431

28. C. C. Tsai, J. T. Bahns, T. J. Whang, H. Wang, W. C. Stwalley, and A. M. Lyyra, *Optical-optical double resonance spectroscopy of the $^1\Sigma_g^+$ ''shelf'' states and $^1\Pi_g$ states of Na_2 using an ultrasensitive ionization detector*, Phys. Rev. Lett. **71**, 1152 (1993). http://doi.org/10.1103/PhysRevLett.71.1152

29. C. C. Tsai, T. J. Whang, J. T. Bahns, and W. C. Stwalley, *The $3\,^1\Sigma_g^+$ ''shelf'' state of Na_2*, Journal of Chemical Physics **99**, 8480 (1993). http://doi.org/10.1063/1.465624

30. C. C. Tsai, J. T. Bahns, and W. C. Stwalley, *Optical–optical double resonance spectroscopy of the $5\,^1\Sigma_g^+$ ''shelf'' state of Na2 using an ultrasensitive ionization detector*, Journal of Chemical Physics **100**, 768 (1994). http://doi.org/10.1063/1.466559

31. C. C. Tsai, J. T. Bahns, H. Wang, T. J. Whang, and W. C. Stwalley, *Optical–optical double resonance spectroscopy of the $4\,^1\Sigma_g^+$ ''shelf'' state of Na_2 using an ultrasensitive ionization detector*, Journal of Chemical Physics **101**, 25 (1994). http://doi.org/10.1063/1.468178

32. T. Laue, P. Pellegrini, O. Dulieu, C. Samuelis, H. Knockel, F. Masnou-Seeuws, and E. Tiemann, *Observation of the long-range potential well of the (6) $^1\Sigma_g^+$ (3s+5s) state of Na_2*, European Physical Journal D **26**, 173 (2003). http://doi.org/10.1140/epjd/e2003-00221-7

33. Y. M. Liu, L. Li, G. Lazarov, A. Lazoudis, A. M. Lyyra, and R. W. Field, *Hyperfine structures of the $2\,^3\Sigma_g^+$, $3\,^3\Sigma_g^+$, and $4\,^3\Sigma_g^+$ states of Na_2*, Journal of Chemical Physics **121**, 5821 (2004). http://doi.org/10.1063/1.1780162

34. L. Li, A. M. Lyyra, W. T. Luh, and W. C. Stwalley, *Observation of the $^{39}K_2$ $a\,^3\Sigma_u^+$ state by perturbation facilitated optical–optical double resonance resolved fluorescence spectroscopy*, Journal of Chemical Physics **93**, 8452 (1990). http://doi.org/10.1063/1.459283

35. C. Amiot, J. Verges, and C. E. Fellows, *The long-range potential of the K_2 $X^1\Sigma_g^+$ ground electronic state up to 15 Å*, Journal of Chemical Physics **103**, 3350 (1995). http://doi.org/10.1063/1.470245

36. J. T. Kim, H. Wang, C. C. Tsai, J. T. Bahns, W. C. Stwalley, G. Jong, and A. M. Lyyra, *Observation of the $4\,^3\Sigma_g^+$, $3\,^3\Pi_g$, $2\,^3\Delta_g$, and $b\,^3\Pi_u$ states of $^{39}K_2$ by perturbation facilitated optical–optical double resonance spectroscopy*, Journal of Chemical Physics **102**, 6646 (1995). http://doi.org/10.1063/1.469137

37. M. R. Manaa, A. J. Ross, F. Martin, P. Crozet, A. M. Lyyra, L. Li, C. Amiot, and T. Bergeman, *Spin-orbit interactions, new spectral data, and deperturbation of the coupled $b\,^3\Pi_u$ and $A\,^1\Sigma_u^+$ states of K_2*, Journal of Chemical Physics **117**, 11208 (2002). http://doi.org/10.1063/1.1522716

38. J. Magnes, E. Ahmed, C. Goldberg, A. M. Lyyra, S. Magnier, M. Aubert-Frecon, Y. M. Liu, and L. Li, *Observation of the K_2 $4\,^3\Delta_g$ state by cw perturbation-facilitated optical-optical double resonance spectroscopy*, Journal of Molecular Spectroscopy **221**, 72 (2003). http://doi.org/10.1016/s0022-2852(03)00177-2

39. E. Ahmed, A. M. Lyyra, F. Xie, D. Li, Y. Chu, L. Li, V. S. Ivanov, V. B. Sovkov, and S. Magnier, *New experimental data on the K_2 $a^3\Sigma_u^+$ state analyzed with the multi-parameter approach*, Journal of Molecular Spectroscopy **234**, 41 (2005). http://doi.org/10.1016/j.jms.2005.08.001

40. Y. Chu, F. Xie, D. Li, L. Li, V. B. Sovkov, V. S. Ivanov, and A. M. Lyyra, *Experimental study of the $^{39}K_2$ $2\,^3\Pi_g$ state by perturbation facilitated infrared-infrared double resonance and two-photon excitation spectroscopy*, Journal of Chemical Physics **122**, 074302 (2005). http://doi.org/10.1063/1.1843815

41. F. Xie, D. Li, L. Li, R. W. Field, and S. Magnier, *Infrared-Infrared double resonance spectroscopy of $^{39}K_2$: The $1\,^3\Delta_g$ state*, Chemical Physics Letters **431**, 267 (2006). http://doi.org/10.1016/j.cplett.2006.10.002

42. S. Falke, I. Sherstov, E. Tiemann, and C. Lisdat, *The $A\,^1\Sigma_u^+$ state of K_2 up to the dissociation limit*, Journal of Chemical Physics **125**, 224303 (2006). http://doi.org/10.1063/1.2375120

43. D. Li, F. Xie, L. Li, V. B. Sovkov, V. S. Ivanov, E. Ahmed, A. M. Lyyra, J. Huennekens, and S. Magnier, *The $^{39}K_2$ $2\,^3\Sigma_g^+$ state: observation and analysis*, Journal of Chemical Physics **126**, 194314 (2007). http://doi.org/10.1063/1.2730804

44. A. Pashov, P. Popov, H. Knockel, and E. Tiemann, *Spectroscopy of the $a\,^3\Sigma_u^+$ state and the coupling to the $X\,^1\Sigma_g^+$ state of K_2*, European Physical Journal D **46**, 241 (2008). http://doi.org/10.1140/epjd/e2007-00307-2

45. C. Amiot and T. S. Carter, *Laser-induced fluorescence of Rb$_2$: The $(1)^1\Sigma_g^+(X)$, $(2)^1\Sigma_g^+$, $(1)^1\Pi_u(B)$, $(1)^1\Pi_g$, and $(2)^1\Pi_u(C)$ electronic states*, The Journal of Chemical Physics **93**, 8591 (1990). http://doi.org/10.1063/1.459246

46. J. D. Miller, R. A. Cline, and D. J. Heinzen, *Photoassociation spectrum of ultracold Rb atoms*, Phys. Rev. Lett. **71**, 2204 (1993). http://doi.org/10.1103/PhysRevLett.71.2204

47. C. Amiot and J. Vergès, *Optical-optical double resonance and Fourier transform spectroscopy: The Rb$_2$ B $^1\Pi_u$ electronic state up to the quasibound energy levels*, Chemical Physics Letters **274**, 91 (1997). http://doi.org/10.1016/S0009-2614(97)00634-9

48. C. Amiot, O. Dulieu, and J. Vergès, *Resolution of the Apparent Disorder of the Rb$_2$ A $^1\Sigma_u^+(0_u^+)$ and b $^3\Pi_u(0_u^+)$ Spectra: A Case of Fully Coupled Electronic States*, Phys. Rev. Lett. **83**, 2316 (1999). http://doi.org/10.1103/PhysRevLett.83.2316

49. J. Y. Seto, R. J. Le Roy, J. Verges, and C. Amiot, *Direct potential fit analysis of the X $^1\Sigma_g^+$ state of Rb$_2$: Nothing else will do!*, Journal of Chemical Physics **113**, 3067 (2000). http://doi.org/10.1063/1.1286979

50. H. Salami, T. Bergeman, B. Beser, J. Bai, E. H. Ahmed, S. Kotochigova, A. M. Lyyra, J. Huennekens, C. Lisdat, A. V. Stolyarov, O. Dulieu, P. Crozet, and A. J. Ross, *Spectroscopic observations, spin-orbit functions, and coupled-channel deperturbation analysis of data on the A $^1\Sigma_u^+$ and b $^3\Pi_u$ states of Rb$_2$*, Phys. Rev. A **80**, 022515 (2009). http://doi.org/10.1103/PhysRevA.80.022515

51. B. Beser, V. B. Sovkov, J. Bai, E. H. Ahmed, C. C. Tsai, F. Xie, L. Li, V. S. Ivanov, and A. M. Lyyra, *Experimental investigation of the ^{85}Rb$_2$ a $^3\Sigma_u^+$ triplet ground state: Multiparameter Morse long range potential analysis*, Journal of Chemical Physics **131**, 094505 (2009). http://doi.org/10.1063/1.3194290

52. Y. Guan, X. Han, J. Yang, Z. Zhou, X. Dai, E. H. Ahmed, A. M. Lyyra, S. Magnier, V. S. Ivanov, A. S. Skublov, and V. B. Sovkov, *Updated potential energy function of the Rb$_2$ $a^3\Sigma_u^+$ state in the attractive and repulsive regions determined from its joint analysis with the $2^3\Pi_{0g}$ state*, Journal of Chemical Physics **139**, 144303 (2013). http://doi.org/10.1063/1.4823496

53. A. N. Drozdova, A. V. Stolyarov, M. Tamanis, R. Ferber, P. Crozet, and A. J. Ross, *Fourier transform spectroscopy and extended deperturbation treatment of the spin-orbit-coupled A $^1\Sigma_u^+$ and b $^3\Pi_u$ states of the Rb$_2$ molecule*, Phys. Rev. A **88**, 022504 (2013). http://doi.org/10.1103/PhysRevA.88.022504

54. X. Han, J. Yang, Y. Guan, Z. Zhou, W. Zhao, A. R. Allouche, S. Magnier, E. H. Ahmed, A. M. Lyyra, and X. Dai, *Observation of the $4^1\Sigma_g^+$ State of Rb$_2$*, Chemical Physics Letters **601**, 124 (2014). http://doi.org/10.1016/j.cplett.2014.04.003

55.   I. Havalyova, A. Pashov, P. Kowalczyk, J. Szczepkowski, and W. Jastrzebski, *The coupled system of $(5)^1\Sigma_u^+$ and $(5)^1\Pi_u$ electronic states in Rb_2*, Journal of Quantitative Spectroscopy and Radiative Transfer **202**, 328 (2017). http://doi.org/https://doi.org/10.1016/j.jqsrt.2017.08.011

56.   A. Pashov, P. Kowalczyk, A. Grochola, J. Szczepkowski, and W. Jastrzebski, *Coupled-channels analysis of the $(5^1\Sigma_u^+,5^1\Pi_u,5^3\Pi_u,2^3\Delta_u)$ complex of electronic states in rubidium dimer*, Journal of Quantitative Spectroscopy and Radiative Transfer **221**, 225 (2018). http://doi.org/https://doi.org/10.1016/j.jqsrt.2018.10.003

57.   A. Pashov, P. Kowalczyk, and W. Jastrzebski, *Double-minimum $3\ ^1\Sigma_u^+$ state in Rb_2: Spectroscopic study and possible applications for cold-physics experiments*, Phys. Rev. A **100**, 012507 (2019). http://doi.org/10.1103/PhysRevA.100.012507

58.   C. Amiot and O. Dulieu, *The Cs_2 ground electronic state by Fourier transform spectroscopy: Dispersion coefficients*, Journal of Chemical Physics **117**, 5155 (2002). http://doi.org/10.1063/1.1499122

59.   F. Xie, V. B. Sovkov, A. M. Lyyra, D. Li, S. Ingram, J. Bai, V. S. Ivanov, S. Magnier, and L. Li, *Experimental investigation of the $Cs_2\ a\ ^3\Sigma_u^+$ triplet ground state: Multiparameter Morse long range potential analysis and molecular constants*, The Journal of Chemical Physics **130**, 051102 (2009). http://doi.org/10.1063/1.3075580

60.   J. A. Coxon and P. G. Hajigeorgiou, *The ground $X\ ^1\Sigma_g^+$ electronic state of the cesium dimer: Application of a direct potential fitting procedure*, Journal of Chemical Physics **132**, 094105 (2010). http://doi.org/10.1063/1.3319739

61.   F. Xie, L. Li, D. Li, V. B. Sovkov, K. V. Minaev, V. S. Ivanov, A. M. Lyyra, and S. Magnier, *Joint analysis of the $Cs_2\ a^3\Sigma_u^+$ and $1_g\ 3^3\Pi_{1g}$ states*, Journal of Chemical Physics **135**, 024303 (2011). http://doi.org/10.1063/1.3606397

62.   S. Sainis, J. Sage, E. Tiesinga, S. Kotochigova, T. Bergeman, and D. DeMille, *Detailed spectroscopy of the $Cs_2\ a^3\Sigma_u^+$ state and implications for measurements sensitive to variation of the electron-proton mass ratio*, Phys. Rev. A **86**, 022513 (2012). http://doi.org/10.1103/PhysRevA.86.022513

63.   A. Znotins, A. Kruzins, M. Tamanis, R. Ferber, E. A. Pazyuk, A. V. Stolyarov, and A. Zaitsevskii, *Fourier-transform spectroscopy, relativistic electronic structure calculation, and coupled-channel deperturbation analysis of the fully mixed $A^1\Sigma_u^+$ and $b\ ^3\Pi_u$ states of Cs_2*, Phys. Rev. A **100**, 042507 (2019). http://doi.org/10.1103/PhysRevA.100.042507

64.   V. B. Sovkov, F. Xie, A. M. Lyyra, E. H. Ahmed, J. Ma, and S. Jia, *Re-examination of the Cs_2 ground singlet $X^1\Sigma_g^+$ and triplet $a^3\Sigma_u^+$ states*, The Journal of Chemical Physics **147**, 104301 (2017). http://doi.org/10.1063/1.5001481

65.   J. Bai, E. H. Ahmed, B. Beser, Y. Guan, S. Kotochigova, A. M. Lyyra, S. Ashman, C. M. Wolfe, J. Huennekens, F. Xie, D. Li, L. Li, M. Tamanis, R. Ferber, A. Drozdova, E. Pazyuk, A. V. Stolyarov, J. G. Danzl, H. C. Nägerl, N. Bouloufa, O. Dulieu, C. Amiot, H. Salami, and T. Bergeman, *Global analysis of data on the spin-orbit-coupled A $^1\Sigma_u^+$ and b $^3\Pi_u$ states of Cs$_2$*, Phys. Rev. A **83**, 032514 (2011). http://doi.org/10.1103/PhysRevA.83.032514

66.   H. Partridge, D. A. Dixon, S. P. Walch, C. W. Bauschlicher, and J. L. Gole, *Electron affinities of the alkali dimers: Na$_2$, K$_2$, and Rb$_2$*, Journal of Chemical Physics **79**, 1859 (1983). http://doi.org/10.1063/1.445962

67.   B. Bussery and M. Aubertfrecon, *Multipolar Long-Range Electrostatic, Dispersion, and Induction Energy Terms for the Interactions Between 2 Identical Alkali Atoms Li, Na, K, Rb, And Cs in Various Electronic States*, Journal of Chemical Physics **82**, 3224 (1985). http://doi.org/10.1063/1.448222

68.   F. Spiegelmann, D. Pavolini, and J. P. Daudey, *Theoretical study of the excited states of the heavier alkali dimers. II. The Rb$_2$ molecule*, Journal of Physics B-Atomic Molecular and Optical Physics **22**, 2465 (1989). http://doi.org/10.1088/0953-4075/22/16/005

69.   M. Krauss and W. J. Stevens, *Effective Core Potentials and Accurate Energy Curves For Cs$_2$ and other Alkali Diatomics*, Journal of Chemical Physics **93**, 4236 (1990). http://doi.org/10.1063/1.458756

70.   M. Foucrault, P. Millie, and J. P. Daudey, *Nonperturbative Method for Core Valence Correlation in Pseudopotential Calculations - Application to the Rb$_2$ And Cs$_2$ Molecules*, Journal of Chemical Physics **96**, 1257 (1992). http://doi.org/10.1063/1.462162

71.   S. Kotochigova, E. Tiesinga, and P. S. Julienne, *Relativistic ab initio treatment of the second-order spin-orbit splitting of the a$^3\Sigma_u^+$ potential of rubidium and cesium dimers*, Phys. Rev. A **63**, 012517 (2001). http://doi.org/10.1103/PhysRevA.63.012517

72.   S. J. Park, S. W. Suh, Y. S. Lee, and G. H. Jeung, *Theoretical study of the electronic states of the Rb$_2$ molecule*, Journal of Molecular Spectroscopy **207**, 129 (2001). http://doi.org/10.1006/jmsp.2001.8337

73.   A. A. Khuskivadze, M. I. Chibisov, and Fabrikant, II, *Adiabatic energy levels and electric dipole moments of Rydberg states of Rb$_2$ and Cs$_2$ dimers*, Phys. Rev. A **66**, 042709 (2002). http://doi.org/10.1103/PhysRevA.66.042709

74.   D. Edvardsson, S. Lunell, and C. M. Marian, *Calculation of potential energy curves for Rb$_2$ including relativistic effects*, Mol. Phys. **101**, 2381 (2003). http://doi.org/10.1080/0026897031000121307

75.   M. Tomza, W. Skomorowski, M. Musial, R. Gonzalez-Ferez, C. P. Koch, and R. Moszynski, *Interatomic potentials, electric properties and spectroscopy of the ground*

and excited states of the Rb$_2$ molecule: ab initio calculations and effect of a non-resonant field, Mol. Phys. **111**, 1781 (2013). http://doi.org/10.1080/00268976.2013.793835

76. W. Jastrzebski, P. Kowalczyk, J. Szczepkowski, A. R. Allouche, P. Crozet, and A. J. Ross, *High-lying electronic states of the rubidium dimer ab initio predictions and experimental observation of the $5^1\Sigma_u^+$ and $5^1\Pi_u$ states of Rb$_2$ by polarization labelling spectroscopy*, Journal of Chemical Physics **143**, 044308 (2015). http://doi.org/10.1063/1.4927225

77. P. T. Arndt, V. B. Sovkov, J. Ma, X. H. Pan, D. S. Beecher, J. Y. Tsai, Y. F. Guan, A. M. Lyyra, and E. H. Ahmed, *The Rb$_2$ $3^1\Pi_g$ state: Observation and analysis*, Journal of Chemical Physics **149**, 224303 (2018). http://doi.org/10.1063/1.5058282

78. P. T. Arndt, V. B. Sovkov, J. Ma, X. H. Pan, D. S. Beecher, J. Y. Tsai, Y. F. Guan, A. M. Lyyra, and E. H. Ahmed, *Experimental study of the $6^1\Sigma_g^+$ state of the rubidium dimer*, Phys. Rev. A **99**, 052511 (2019). http://doi.org/10.1103/PhysRevA.99.052511

79. J. R. d. Laeter, J. K. Böhlke, P. D. Bièvre, H. Hidaka, H. S. Peiser, K. J. R. Rosman, and P. D. P. Taylor, *Atomic weights of the elements. Review 2000 (IUPAC Technical Report)*, Pure and Applied Chemistry **75**, 683 (2003). http://doi.org/doi:10.1351/pac200375060683

80. C. R. Vidal and J. Cooper, *Heat-Pipe Oven - a New, Well-Defined Metal Vapor Device for Spectroscopic Measurements*, J. Appl. Phys. **40**, 3370 (1969). http://doi.org/10.1063/1.1658190

81. A. N. Nesmeyanov, *Vapor Pressure of the Chemical Elements* (Elsevier, 1963).

82. W. Demtröder, *Laser Spectroscopy - Basic Concepts and Instrumentation* (Springer, 2003).

83. J. E. Sansonetti, *Wavelengths, transition probabilities, and energy levels for the spectra of rubidium (RbI through RbXXXVII)*, Journal of Physical and Chemical Reference Data **35**, 301 (2006). http://doi.org/10.1063/1.2035727

84. X. B. Xie and R. W. Field, *Perturbation Facilitated Optical-Optical Double Resonance spectroscopy of the $^6Li_2$ $3^3\Sigma_g^+$, $2^3\Pi_g$, $1^3\Delta_g$, $b^3\Pi_u$, and $a^3\Sigma_u^+$ state*, Journal of Molecular Spectroscopy **117**, 228 (1986). http://doi.org/10.1016/0022-2852(86)90152-9

85. B. A. Palmer, R. A. Keller, and R. Engleman, *An Atlas of Uranium Emission Intensities in a Hollow Cathode Discharge* (Los Alamos Scientific Laboratory, New Mexico, 1980).

86. R. A. Keller, R. Engleman, and B. A. Palmer, *Atlas for optogalvanic wavelength calibration*, Applied Optics **19**, 836 (1980). http://doi.org/10.1364/ao.19.000836

87. P. F. Bernath, *Spectra of atoms and molecules* (Oxford University Press, New York; Oxford, 2005).

88. S. Gerstenkorn and P. Luc, *Atlas of the Absorption Spectra of Molecular Iodine for 14,800 cm^{-1} to 20,000 cm^{-1}* (CNRS, Paris, 1978).

89. S. Gerstenkorn and P. Luc, *Absolute Iodine I_2 Standards Measured by Means of Fourier-Transform Spectroscopy*, Revue De Physique Appliquee **14**, 791 (1979). http://doi.org/10.1051/rphysap:01979001408079100

90. E. J. Breford and F. Engelke, *Laser-induced molecular fluorescence in supersonic nozzle beams: Applications to the NaK D $^1\Pi$ - X $^1\Sigma^+$ and D $^1\Pi$ - $a^3\Sigma^+$ systems*, Chemical Physics Letters **53**, 282 (1978). http://doi.org/10.1016/0009-2614(78)85397-4

91. E. U. Condon, *Nuclear motions associated with electron transitions in diatomic molecules*, Physical Review **32**, 0858 (1928). http://doi.org/10.1103/PhysRev.32.858

92. G. Herzberg, *Spectra of Diatomic Molecules* (Van Nostrand, New York, 1950).

93. J. X. Yang, W. Zhao, X. H. Pan, H. M. Wei, J. Ma, E. H. Ahmed, A. M. Lyyra, and X. C. Dai, *Experimental study of the $b^3\Pi_{1u}$ and $2^3\Pi_{1g}$ states of $^{85}Rb_2$*, Journal of Molecular Spectroscopy **336**, 36 (2017). http://doi.org/10.1016/j.jms.2017.04.011

94. L. Li, Q. S. Zhu, A. M. Lyyra, T. J. Whang, W. C. Stwalley, R. W. Field, and M. H. Alexander, *Collision-Induced Transitions between $A^1\Sigma_u^+$ and $b\ ^3\Pi_u$ states of Na_2 - the gateway effect of perturbed levels*, Journal of Chemical Physics **97**, 8835 (1992). http://doi.org/10.1063/1.463971

95. Y. Gao, P. S. Gorgone, S. Davis, E. K. McCall, and B. Stewart, *Dependence of level-resolved energy transfer on initial vibrational level in $Li_2\,A^1\Sigma_u^+ - Ne$ collisions*, The Journal of Chemical Physics **104**, 1415 (1996). http://doi.org/10.1063/1.470908

96. L. Li, S. Antonova, A. Yiannopoulou, K. Urbanski, and A. M. Lyyra, *State-to-state collision energy transfer of $^7Li_2$ within high-lying triplet states: Gateway effect of mixed levels in energy transfer between singlet and triplet states*, Journal of Chemical Physics **105**, 9859 (1996). http://doi.org/10.1063/1.472852

97. C. Ottinger, R. Velasco, and R. N. Zare, *Some Propensity Rules in Collision- Induced Rotational Quantum Jumps*, The Journal of Chemical Physics **52**, 1636 (1970). http://doi.org/10.1063/1.1673198

98. Vladimir B. Sovkov and J. Ma, in *Advances in Computer Science Research: Proceedings of the 2016 International Conference on Applied Mathematics, Simulation and Modelling* (Atlantis Press, Beijing, 2016), p. 369.

99. V. B. Sovkov, in *Optimizer: source codes and manuals & collection of applications*.

100. S. S. Onishchenko, V. B. Sovkov, F. Xie, D. Li, S. S. Lukashov, V. V. Baturo, J. Wu, J. Ma, and L. Li, *Analysis of the hyperfine structure of the $Cs_2\ 3^3\Sigma_g^+$ state*, Journal of Quantitative Spectroscopy and Radiative Transfer **250**, 107037 (2020). http://doi.org/https://doi.org/10.1016/j.jqsrt.2020.107037

101. X. Wang, W. Liu, Y. Li, J. Wu, V. B. Sovkov, J. Ma, S. Onishchenko, P. Li, Y. Fu, D. Li, Q. Fan, L. Xiao, and S. Jia, *Hyperfine structure of the NaCs $b^3\Pi_2$ state near the dissociation limit $3S_{1/2} + 6P_{3/2}$ observed with ultracold atomic photoassociation*, Physical Chemistry Chemical Physics **22**, 3809 (2020). http://doi.org/10.1039/c9cp05870b

102. S. S. Onishchenko, V. B. Sovkov, F. Xie, D. Li, S. S. Lukashov, V. V. Baturo, J. Wu, and J. Ma, *Analysis of the hyperfine structure of the 13Δg, 23Πg, and 33Σg+ states of 6Li7Li*, Journal of Quantitative Spectroscopy and Radiative Transfer **270**, 107665 (2021). http://doi.org/10.1016/j.jqsrt.2021.107665

103. J. L. Dunham, *The energy levels of a rotating vibrator*, Physical Review **41**, 721 (1932). http://doi.org/10.1103/PhysRev.41.721

104. R. Rydberg, *Graphical Representation of some bound spectroscopic Results*, Z. Physik **73**, 376 (1932). http://doi.org/10.1007/bf01341146

105. R. Rydberg, *Some potential curves of mercury hydrides*, Z. Physik **80**, 514 (1933). http://doi.org/10.1007/bf02057312

106. O. Klein, *For the calculation of potential curves for diatomic molecules with spectral help*, Z. Physik **76**, 226 (1932). http://doi.org/10.1007/bf01341814

107. A. L. G. Rees, *The calculation of potential-energy curves from band-spectroscopic data*, Proceedings of the Physical Society of London **59**, 998 (1947). http://doi.org/10.1088/0959-5309/59/6/310

108. J. Tellinghuisen, *A direct potential fitting RKR method: Semiclassical vs. quantal comparisons*, Journal of Molecular Spectroscopy **330**, 20 (2016). http://doi.org/10.1016/j.jms.2016.09.008

109. E. W. Kaiser, *Dipole Moment and Hyperfine Parameters of $H^{35}Cl$ and $D^{35}Cl$*, The Journal of Chemical Physics **53**, 1686 (1970). http://doi.org/10.1063/1.1674245

110. P. Qi, J. Bai, E. Ahmed, A. M. Lyyra, S. Kotochigova, A. J. Ross, C. Effantin, P. Zalicki, J. Vigue, G. Chawla, R. W. Field, T. J. Whang, W. C. Stwalley, H. Knockel, E. Tiemann, J. Shang, L. Li, and T. Bergeman, *New spectroscopic data, spin-orbit functions, and global analysis of data on the $A\ ^1\Sigma_u^+$ and $b^3\Pi_u$ states of Na_2*, Journal of Chemical Physics **127**, 044301 (2007). http://doi.org/10.1063/1.2747595

111. J. Zaharova, M. Tamanis, R. Ferber, A. N. Drozdova, E. A. Pazyuk, and A. V. Stolyarov, *Solution of the fully-mixed-state problem: Direct deperturbation analysis of the $A^1\Sigma^+ - b^3\Pi$ complex in a NaCs dimer*, Phys. Rev. A **79**, 012508 (2009). http://doi.org/10.1103/PhysRevA.79.012508

112. A. W. Mantz, J. K. G. Watson, K. N. Rao, D. L. Albritton, A. L. Schmeltekopf, and R. N. Zare, *Rydberg-Klein-Rees potential for the $X^1\Sigma^+$ state of the CO molecule*, Journal of Molecular Spectroscopy **39**, 180 (1971). http://doi.org/10.1016/0022-2852(71)90292-X

113. J. K. G. Watson, *The isotope dependence of diatomic Dunham coefficients*, Journal of Molecular Spectroscopy **80**, 411 (1980). http://doi.org/10.1016/0022-2852(80)90152-6

114. V. G. Tyuterev and T. I. Velichko, *High-order anharmonicity parameters in various representations of the diatomic potential function and exact relations between spectroscopic constants. application to the co molecule*, Chemical Physics Letters **104**, 596 (1984). http://doi.org/10.1016/0009-2614(84)80035-4